Advancing Aluminum Casting Optimization With Real-Time Temperature and Gap Measurements Using Optical Fiber Sensors at the Metal-Mold Interface

Bohong Zhang, *Member, IEEE*, Abhishek Prakash Hungund, Dinesh Reddy Alla, Deva Prasaad Neelakandan, Muhammad Roman, Ronald J. O'Malley, Laura Bartlett, Rex E. Gerald II, and Jie Huang, *Senior Member, IEEE*

***Abstract*— Accurate measurement of interfacial heat transfer during casting solidification is crucial for optimizing metal solidification processes. The gap between the mold wall and the casting surface plays a significant role in heat transfer and cooling rates. In this study, two innovative fiber-optic sensors are employed to measure real-time mold gaps and thermal profiles during the solidification of A356 aluminum in a permanent mold casting. The experimental setup consists of a specially designed mold system made of unheated, uncoated tool steel, which facilitates easy installation of the fiber-optic sensors. An Extrinsic Fabry–Perot interferometric (EFPI) sensor is utilized to monitor the evolving gap between the mold wall and the casting surface. This method relies on the unique concept of using molten metal as the second reflection interface for gap measurements. The EFPI gap measurements exhibit high accuracy and precision, with a maximum error of only 2 μm when compared to physical measurements. Simultaneously, a stainless steel-encased fiber utilizing the Rayleigh backscattering (RBS) technique is deployed across the mold wall and cavity to achieve real-time temperature measurements with a spatial resolution of 0.65 mm. The study demonstrates that leveraging high-resolution temperature profiles and gap evolution measurements enhances understanding of heat transfer dynamics at the mold-metal interface, particularly valuable for complex-shaped castings and continuously cast metals. Additionally, the ability to measure the cast shape exiting a continuous casting mold during operation presents a novel tool for real-time product quality monitoring and process safety enhancement by detecting conditions that may lead to slab cracking and breakouts.**

***Index Terms*— Aluminum casting, distributed temperature measurement, extrinsic Fabry–Perot interferometer (EFPI), gap measurement, interfacial heat transfer, molten metal, optical fiber sensors, optical frequency-domain reflectometry (OFDR), Rayleigh backscattering (RBS).**

I. Introduction

SOLIDIFICATION is a fundamental step in metal production, involving the transformation of liquid metal into a desired solid shape [1], [2]. The use of molds is prevalent in this process, as they play a crucial role in shaping the metal. However, the heat transfer dynamics at the mold-metal interface, particularly for complex-shaped castings and continuously cast metals, remain poorly understood [3], [4]. To bridge this knowledge gap, mathematical models integrating solidification, heat transfer, and mechanical stress have been employed to enhance our understanding of the interface gap during solidification in static molds [5], [6], [7]. These models consider factors such as cooling rate and temperature gradients between the mold and metal, providing valuable insights into solidification and opportunities for process optimization. Similarly, advanced models have been developed to simulate heat transfer and solidification in continuous casting molds [3], [8], [9], [10]. These models account for factors such as the liquid and crystalline layers of mold flux in the gap, as well as the movement of the mold itself. By incorporating these factors, a comprehensive understanding of mold flux behavior and heat transfer can be achieved. A thorough understanding of metal solidification is crucial for achieving better control, consistency, and higher-quality metals. These models have significantly improved metal manufacturing processes by enhancing efficiency, reducing costs, and improving the quality of the final product. By leveraging scientific models to explore the complexities of solidification, we can gain valuable insights and develop more efficient and effective manufacturing processes.

Enhancing metal manufacturing processes often involves the direct measurement of mold gaps and temperature profiles

Manuscript received 26 June 2023; revised 19 September 2023; accepted 20 October 2023. Date of publication 1 November 2023; date of current version 14 November 2023. This was supported in part by the Defense Logistics Agency (DLA)-Troop Support, Philadelphia, PA, USA; in part by the Defense Logistics Agency Information Operations, J68, Research and Development, Ft. Belvoir, VA, USA; in part by the U.S. Department of Energy's Office of Energy Efficiency and Renewable Energy (EERE) under the Advanced Manufacturing Office (AMO) under Award DE-EE0009119; and in part by the Peaslee Steel Manufacturing Research Center (PSMRC) at the Missouri University of Science and Technology, Rolla, MO, USA. The Associate Editor coordinating the review process was Dr. Yuhua Chen. *(Bohong Zhang and Abhishek Prakash Hungund contributed equally to this work.) (Corresponding author: Jie Huang.)*

Bohong Zhang, Abhishek Prakash Hungund, Dinesh Reddy Alla, Muhammad Roman, Rex E. Gerald II, and Jie Huang are with the Department of Electrical and Computer Engineering, Missouri University of Science and Technology, Rolla, MO 65409 USA (e-mail: jieh@mst.edu).

Deva Prasaad Neelakandan, Ronald J. O'Malley, and Laura Bartlett are with the Department of Materials and Science Engineering, Missouri University of Science and Technology, Rolla, MO 65409 USA.

Digital Object Identifier 10.1109/TIM.2023.3329217

during high-temperature solidification. Linear displacement sensors, particularly linear variable differential transformers (LVDTs) [11], [12], [13], have been widely employed for this purpose. LVDTs offer a linear output and excellent resolution, enabling highly accurate measurements down to a few microns. Their advantages include low friction and extended lifespan, making them reliable for applications requiring precise linear displacement measurements. However, it is important to acknowledge some drawbacks associated with LVDTs. LVDTs can be relatively expensive compared to other displacement sensors and require signal conditioning electronics. They are also sensitive to environmental factors such as temperature changes, and external magnetic fields can introduce measurement errors. Despite these limitations, LVDTs are still popular in various industries, including automotive, aerospace, and industrial sectors [14], [15], [16]. To mitigate the influence of external factors, effective measures can be taken when using LVDTs. These include shielding or enclosing them and employing signal conditioning electronics to amplify and filter the output signal. However, challenges arise in the steelmaking industry due to the mechanical complexity of LVDTs and the need for temperature compensation, limiting their application in this field. Fortunately, there have been promising advancements in the form of emerging techniques, such as fiber-optic sensors, which show potential for overcoming these limitations. Fiber-optic sensors offer new avenues for more accurate and reliable measurements in the solidification process. Unlike LVDTs, fiber-optic sensors are immune to electromagnetic interference and can operate in harsh environments. They can also provide distributed sensing capabilities along the fiber, allowing for simultaneous measurement of multiple points. The utilization of fiber-optic sensors in measuring mold gaps and temperature profiles during solidification presents exciting possibilities for improved accuracy and reliability. By leveraging the unique advantages of fiber-optic technology, such as immunity to electromagnetic interference and distributed sensing capabilities, these sensors hold promise for enhancing solidification processes in various industries, including steelmaking.

Fiber-optic sensors have emerged as a highly promising technology with increasing adoption across various industries in recent decades. These sensors utilize light to detect and measure environmental changes, endowing them with exceptional sensitivity and selectivity. Their applications span a wide range of fields, including civil engineering for structural health monitoring and healthcare and industry for biomedical sensing [17], [18], [19], [20]. Notably, one of the key advantages of fiber-optic sensors lies in their ability to operate reliably in harsh and hazardous environments [21], [22], [23], [24]. Unlike traditional sensors containing electrical components, fiber-optic sensors can withstand extreme temperatures, radiation, and high pressures that would render conventional sensors unsuitable. Furthermore, fiber-optic sensors are immune to electromagnetic interference, making them well-suited for use in electromagnetic fields. The accuracy of fiber-optic sensors is another notable advantage, enabling precise detection of temperature and strain changes [25], [26], [27]. This precision makes them highly attractive to manufacturers requiring tight process control to ensure product quality and production efficiency. In summary, fiber-optic sensors possess significant potential across a wide range of industries, including healthcare, civil engineering, and steel engineering. Their exceptional sensitivity, accuracy, and ability to operate in harsh environments make them an appealing choice. While specialized expertise is necessary for optimal performance, the impressive capabilities and versatility of fiber-optic sensors make them an increasingly preferred option for numerous applications.

In this article, we present experimental findings utilizing a temperature-insensitive optical fiber Fabry–Perot interferometer (FPI) approach for dynamic measurements of the mold gap at elevated temperatures during the casting process. A novel concept is introduced, employing molten metal as the second reflection interface for gap measurements, which offers accurate and real-time detection of gap changes during liquid metal solidification. This approach provides valuable insights into the metal solidification process. The obtained gap measurements are compared with physical measurements, demonstrating highly accurate and precise results with a mere 2 μm error. Additionally, we utilize the RBS technique to develop a novel method for measuring temperature distributions across the mold cavity and walls during aluminum solidification. By inserting a single channel single-mode optical fiber into a stainless-steel tube, we achieve temperature monitoring across the mold wall and cavity with an impressive spatial resolution of 0.65 mm. These temperature measurements enable the creation of a comprehensive thermal profile, shedding light on heat transfer dynamics throughout the entire molten aluminum solidification process. The direct measurement of the mold gap and temperature profile across the gap holds significant potential for the metal industry, such as continuous casting, hot rolling, and steel forging. It allows for enhanced control and optimization of the solidification process, leading to substantial improvements in product quality and consistency. Moreover, this approach has implications beyond the realm of quality control. It has the potential to facilitate the development of new alloys, simplifying the production of previously challenging-to-cast alloys within existing manufacturing processes. This advancement holds promise for both military and industrial markets, enabling the production of more sophisticated and specialized alloy products. In summary, our findings highlight the successful utilization of a temperature insensitive FPI approach for dynamic mold gap measurements and the innovative use of molten metal as a reflection interface. Additionally, we demonstrate the applicability of the RBS technique for temperature monitoring during aluminum solidification. This development significantly impacts the metal industry, offering improved control, optimized solidification, and enhanced product quality. Furthermore, it opens doors to new alloy possibilities and greater manufacturing efficiency.

II. Sensing Mechanism

A. Fabry–Perot Interferometer

FPI is a widely employed optical measurement tool that relies on the interference of light waves [28]. It comprises a

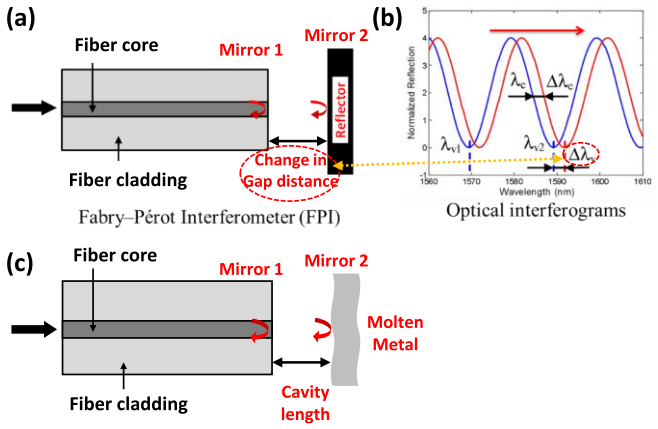

Fig. 1. Sensing principle and interferograms of an optical fiber EFPI. (a) EFPI cavity is formed by placing two reflective mirrors at the ends of a single-mode optical fiber, creating a cavity with a specific length. When a broadband light source is coupled into the fiber, the reflected light from the mirrors interferes, resulting in a pattern of interference fringes. (b) Changes in the cavity length caused by external perturbations, such as pressure or temperature variations, cause a shift in the interference pattern, enabling precise measurement of the perturbation. (c) In this study, a novel approach utilizing molten metal as the second mirror was proposed for the first time and implemented for monitoring gap changes during the solidification of aluminum in a mold.

pair of flat, parallel mirrors separated by a known distance. Incident light waves are reflected back and forth between these mirrors, resulting in interference patterns as the waves interact. Analyzing these interference patterns provides valuable information about the physical properties of the system being studied. FPIs are versatile and capable of measuring various physical phenomena, including temperature, pressure, strain, and refractive index [17], [29], [30]. They exhibit high sensitivity and selectivity and can capture both static and dynamic changes in the environment. The performance of FPIs can be enhanced through different techniques. For instance, the inclusion of multiple mirrors or the incorporation of wavelength tuning sources like piezoelectric transducers or tunable lasers can improve the instrument's resolution and range. These techniques augment the capabilities of FPIs, making them invaluable for scientific and industrial applications. In the field of optical metrology, FPIs serve as a vital tool, delivering precise and reliable measurements for a wide range of physical parameters. Fig. 1(a) and (b) illustrates the working principle and the optical interferograms of an optical fiber FPI, respectively.

The endface of the optical fiber and a second reflector form an EFPI with a cavity length of L. The resulting interference signal I is given by

$$I = I_1 + I_2 + 2\sqrt{I_1 I_2}\cos\left(\frac{4\pi nL}{\lambda} + \varphi\right) \tag{1}$$

where I_1 and I_2 represent the light intensities reflected from the endface of the optical fiber and a second reflector, respectively. Additionally, φ denotes the initial phase difference of the interferometer, n represents the refractive index of air as 1.0000293 (approximately 1), and L indicates the length of the air cavity [17], [30], [37]. The change in the refractive index of air from room temperature to high temperature is typically small, with minimal impact on most experiments [36]. This change is usually on the order of 10^{-6}/°C. In practical applications and experiments, including this study, this change is considered negligible and can be effectively managed through calibration or compensation methods. The free spectral range (FSR) is the distance between two successive minima in the interferogram. The FSR can be calculated using the following equation as:

$$\mathrm{FSR} = \frac{\lambda^2}{2L} \tag{2}$$

where λ is the wavelength of the propagated light [37]. So, the cavity length can be demodulated by determining the FSR of the interferogram. The change in cavity length ΔL can be determined by

$$\Delta L = \frac{\lambda^2 \Delta \mathrm{FSR}}{\mathrm{FSR}_1 \mathrm{FSR}_2} \tag{3}$$

where FSR_1 and FSR_2 are the values of FSR before and after displacement, respectively [37].

In this study, we introduce a novel method utilizing an optical fiber EFPI as a sensing element to monitor gap changes during aluminum solidification, as depicted in Fig. 1(c). The endface of the single-mode fiber acts as the first reflector, while the molten aluminum acts as the second reflector. As the molten aluminum undergoes solidification, the optical cavity length increases proportionally, allowing direct measurement of the shrinkage process. Notably, the optical cavity length exhibits a plateau toward the end of the solidification process, which offers valuable insights into process dynamics. This plateau represents a critical point where the molten aluminum transitions from a liquid to a solid state, resulting in shrinkage. By experimentally monitoring the gap changes during aluminum solidification (shrinkage), we gain a deeper understanding of the underlying physics and develop computer models that can optimize the casting process and enhance the quality of the final product. The findings of this study represent a significant advancement in the monitoring, prediction, and control of the casting process, paving the way for improved casting methodologies and enhanced product quality.

B. Rayleigh Backscattering (RBS)

RBS refers to the phenomenon where light or electromagnetic radiation is scattered by particles that are significantly smaller than the wavelength of the radiation [31]. Specifically, it describes the scattering of radiation that is directed back toward the source rather than being scattered in other directions. RBS finds diverse applications in industries such as telecommunications, remote sensing, and environmental monitoring [32], [33]. In optical fiber communication systems, RBS is a prominent source of noise. However, by analyzing the characteristics of the backscattered signal, valuable information about the fiber and its environment can be extracted. Lidar systems utilize RBS to measure atmospheric conditions, while it is also employed for air pollution detection and monitoring particulate matter concentrations in environmental applications [34]. RBS serves as a sensing mechanism for temperature measurement in optical fibers [35]. The proposed

system for distributed temperature measurements relies on the phenomenon of Rayleigh scattering within a single-mode optical fiber. Rayleigh scattering occurs when incident light interacts with discontinuities in a medium characterized by dimensions smaller than the wavelength of the incident light. Within the context of an optical fiber, random fluctuations in the refractive index of the fiber material give rise to Rayleigh scattering phenomena. Temperature fluctuations induce alterations in both the refractive index and the physical length of the optical fiber, thereby inducing discernible spectral shifts in the RBS spectra. Using RBS for temperature measurement offers several advantages, including high accuracy, high sensitivity, and the ability to measure temperature at multiple points along a single fiber. Moreover, it is a noninvasive technique that does not require physical contact with the fiber, making it well-suited for harsh environments or applications where accessing the fiber is challenging.

This study introduces a novel method for measuring temperature distributions during aluminum solidification across a mold cavity and mold walls. To achieve this, an optical fiber, encased in a stainless-steel tube, was employed for temperature measurements with high spatial resolution and a rapid measurement acquisition rate. The measurement technique relied on RBS using a coating-stripped single-mode optical fiber with an outer diameter of 0.125 mm. Temperature changes induce modifications in the refractive index and length of the optical fiber, leading to shifts in the RBS signal. By monitoring these shifts, temperature variations can be accurately measured and mapped across the mold cavity and walls during the solidification process. This innovative approach provides valuable insights into the thermal dynamics and behavior of the aluminum solidification process, facilitating process optimization and enhancing the quality of the final product. The RBS shift $\Delta\lambda$ resulting from a temperature change ΔT is expressed as

$$\Delta\lambda = \lambda(\alpha + \zeta)\Delta T \tag{4}$$

where λ is the operating wavelength, α is the thermal expansion coefficient (0.55×10^{-6}/°C), and ζ is the thermo-optic coefficient (8.5×10^{-6}/°C) of the optical fiber [35]. The reference RBS signal from the fiber under test was initially recorded when the fiber was placed in the test setup at room temperature. Subsequently, Rayleigh signals obtained at elevated temperatures were compared to the reference signal using cross correlation analysis. This comparison allowed for the measurement of spectrum shifts, which were then converted into temperature measurements using temperature coefficients specific to the fiber material. By utilizing this methodology, accurate and precise temperature measurements were obtained, enabling a comprehensive understanding of temperature variations during the experiment. The RBS signals were acquired and processed using an interrogator based on optical frequency-domain reflectometry (OFDR). OFDR is an optical sensing technique employed for measuring physical properties, including temperature and strain, along an optical fiber. It utilizes a swept coherent light source to inject light into the fiber. As the light propagates through the fiber, a small fraction is backscattered due to microscopic variations

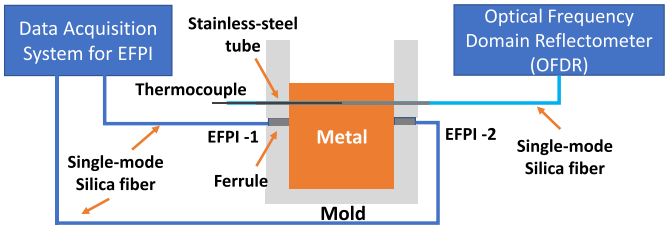

Fig. 2. Schematic of the experimental setup for aluminum casting. Two EFPIs are embedded on opposite sides of the mold wall and connected to the integrator for data acquisition. The RBS-instrumented channel is positioned across the mold wall and cavity, and it is connected to the OFDR integrator for temperature monitoring.

in the refractive index, leading to Rayleigh scattering. The backscattered light carries information about the fiber's physical properties, such as temperature. OFDR measures these properties by analyzing the interference between the incident light and the backscattered light at different positions along the fiber. This analysis involves comparing the phase and intensity of the reference signal with the backscattered light at different frequencies, resulting in interference patterns. These patterns are then transformed from the frequency domain to the distance domain using Fourier transform. The resulting high-resolution profile of the backscattered light provides valuable insights into the distribution of backscattered light intensity, enabling the detection and localization of temperature or strain changes along the fiber with exceptional precision. In this study, temperature measurements were performed using OFDR with a remarkable spatial resolution of 0.65 mm and a rapid measurement acquisition rate of 13 Hz. This allowed for the detailed characterization of temperature distributions during the aluminum solidification process. The innovative method employed in this research has significant potential for advancing the field of materials science and industry, as it enables more accurate and efficient temperature measurements during solidification processes. It offers valuable insights into the thermal dynamics and behavior of the process, facilitating improved process optimization and enhanced product quality.

III. Experimental

A. Experimental Setup and Sensors Installation

The positioning of the EFPI sensor inside a ferrule and its installation through the mold wall are illustrated in Fig. 2. To ensure proper alignment and secure the fibers in place, the cleaved EFPI fibers are placed within the ferrule. The ferrule is then fixed to the mold wall using refractory cement, ensuring the accuracy of gap measurements during the solidification process. Care was taken to select a precision collar hole diameter that minimizes metal penetration while the mold is being filled. When liquid metal is poured into the mold, a reflective surface is formed. As the metal gradually cools and solidifies, it undergoes shrinkage, which can be precisely measured using the EFPI sensor. This measurement allows for the determination of the gap between the reflective surface and the sensor. The accurate measurement of this gap is essential for understanding and analyzing the interfacial heat transfer that occurs during solidification. The insights gained from

this measurement contribute to the improved understanding of casting processes and aid in enhancing the accuracy of interfacial heat transfer models. A coating-stripped single-mode optical fiber with an outer diameter of 0.125 mm was employed to measure temperature changes using RBS. In order to mitigate potential mechanical distortions caused by delamination and combustion of the polymer coating, the coating was intentionally removed. To safeguard the fragile fiber from mechanical impacts, it was enclosed within a stainless-steel tube positioned across the mold wall and cavity. It is important to note that while the stainless-steel tube provides mechanical protection, its primary purpose is not to shield against the variables (temperature, strain/pressure) being measured. RBS served as the basis for temperature measurement, where alterations in the refractive index and length of the optical fiber led to shifts in the RBS signal. The temperature measurements obtained from the OFDR system were processed and discussed in detail. To establish a reference temperature at the center of the mold cavity, a K-type thermocouple was also placed inside the stainless-steel tube alongside the RBS channel, as depicted in Fig. 2. This reference temperature served as a comparison point for the optical fiber temperature measurements taken at the same location. By comparing the temperature readings from the thermocouple and the optical fiber, the accuracy of temperature measurements during the mold filling process could be verified and ensured.

B. Mold Design

To facilitate the installation of the optical fiber sensors into the mold walls and through the mold cavity, a permanent mold system made of unheated, uncoated tool steel was designed. The mold cavity had a width of 25.4 mm, specifically accommodating the placement of the fiber-optic sensors. The detailed dimensions and design of the mold are presented in Fig. 3. During the experiments, commercial-grade molten A356 aluminum was poured into the non-preheated, permanent mold system, which was equipped with two types of sensor port holes. The first hole type housed an optical fiber equipped with RBS technology for temperature measurements, while the second hole type contained a ferrule that encapsulated an EFPI sensor for gap measurements, as illustrated in Fig. 3(a) and (b). This mold design ensured precise sensor placement within the mold, enabling real-time measurements of the gap between the mold wall and the casting surface, as well as the temperature distribution across the interior mold walls. By employing this mold design, casting experiments were conducted to obtain crucial data on the gap between the mold wall and the casting surface, as well as the temperature distribution across a critical dimension of the mold. These measurements provide essential insights for enhancing the understanding of casting processes and improving the accuracy of interfacial heat transfer computer models, ultimately advancing the optimization and control of the casting process.

C. Preliminary Sensor Calibration

Before conducting the casting experiments, the advanced EFPI sensors underwent comprehensive calibration testing.

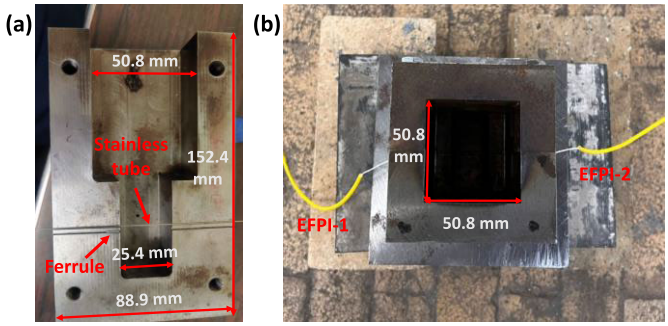

Fig. 3. Images of the instrumented mold and sensor placements. (a) Cross–sectional view of the designed mold, highlighting the stainless-steel tube used for RBS temperature measurement across the mold wall and cavity, and the ferrule employed for the left side EFPI channel. The upper mold cavity spans 50.8 mm, while the bottom cavity measures 25.4 mm. (b) Top view of the instrumented mold, demonstrating the installation of two EFPIs, one on the left and one on the right side.

To determine their accuracy, a highly reflective metal mirror attached to a micrometer was employed as a reference standard, as depicted in Fig. 4. The mirror was placed on an automatic horizontal micrometer stage that allowed for linear movement with a resolution below 1 μm, as shown in Fig. 4(a). The stage was programmed to move in intervals of 25 μm for the initial 50 μm displacement (two steps), followed by 50 μm intervals for the remaining 950 μm displacement (20 steps). Throughout the calibration experiment, a total of 23 measurements were taken. The cavity length values obtained from the Bay-spec integrator were compared with the displacement values measured by the micrometer, and the results are presented in Fig. 4(b). A linear fitting function was applied to the collected data to evaluate the reliability of the measurements. The linear fit yielded a slope value of 0.9932, indicating a high level of measurement accuracy for the EFPI sensors. This finding is of great significance as it demonstrates the suitability of the sensors for applications that require highly precise measurements. Furthermore, the linear relationship observed between the micrometer displacement and the estimated cavity length values highlights the consistency and reliability of the EFPI sensors. This consistency is crucial for applications that demand precise measurements to ensure the accuracy and quality of the final product.

The accuracy of monitoring the gap during casting is of utmost importance, and to achieve this, an advanced EFPI sensor is utilized. A sensor installation calibration was conducted to ensure the accuracy of the gap measurements, as depicted in Fig. 5. Initially, the bare cleaved fiber was placed within a ferrule to align and secure the fiber. Subsequently, the ferrule was securely fixed to the mold wall, first using superglue to immobilize the ferrule and then refractory cement to fix the ferrule in place permanently, preventing any movement during the solidification process. To avoid any potential damage caused by the ferrule coming into contact with the molten aluminum, an offset was introduced during the ferrule installation. Fig. 5(a) presents a detailed schematic of the EFPI setup within the designed mold. The labels "*a*," "*b*," and "*c*" indicate the offset between the fiber end face and the mold wall, the distance between the fiber end face

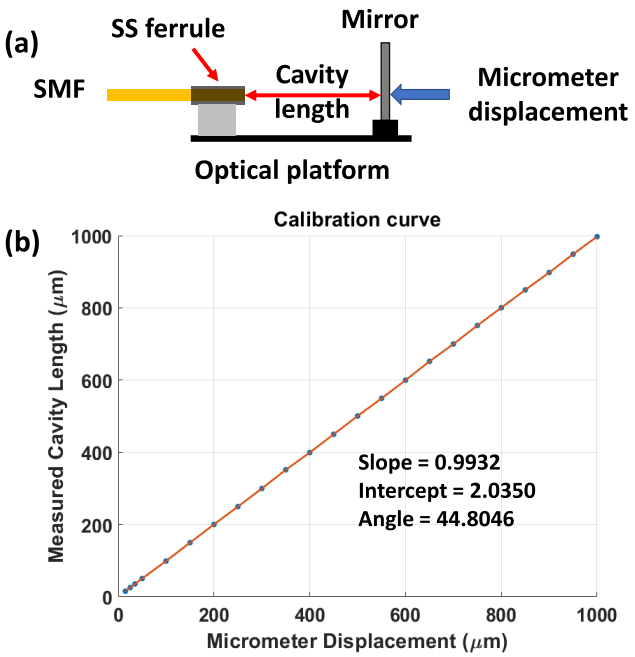

Fig. 4. Calibration setup and results of the EFPI-based instrument for measuring gaps. (a) Graph demonstrates the calibration test conducted by horizontally moving the mirror in 25- and 50-μm increments, as depicted in the figure insert. (b) Orange line represents the linear regression of the data points, exhibiting a calculated slope of 0.9932, indicative of high measurement accuracy.

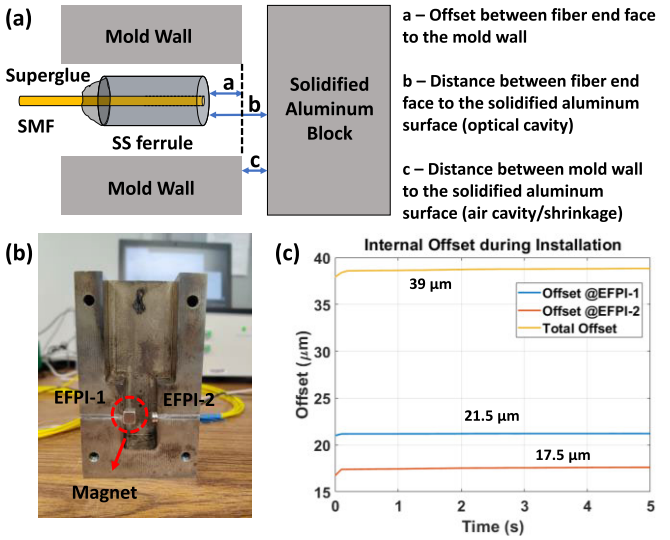

Fig. 5. EFPI installation offset calibration test and results using a magnet with a mirror surface. (a) Image of the calibration experiment setup showcasing a magnet with a mirror surface attached to the inner mold wall for offset measurement. (b) Graph displaying the offset calibration results for two EFPI channels, demonstrating that the offsets for both channels were measured to be below 22 μm. (c) Experimental results of internal offset during installation.

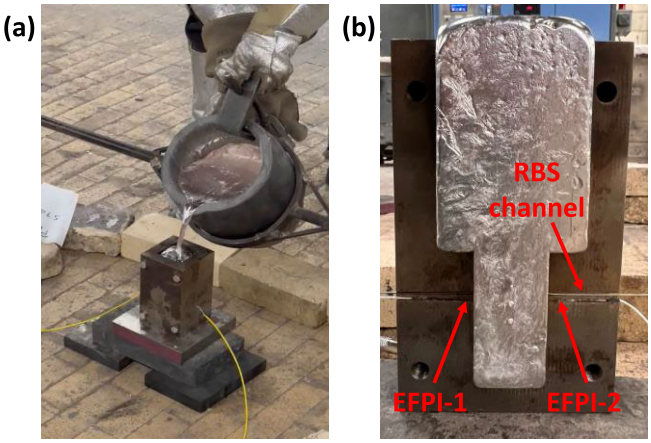

Fig. 6. Images of the aluminum pouring experiment. (a) Molten aluminum liquid at 650 °C is poured into the designed mold, filling the inner cavity. (b) Image of the solidified aluminum sample with RBS and two EFPI channels embedded, illustrating the successful completion of the experiment without any damage to the sensor channels.

and the solidified aluminum surface (the optical cavity), and the distance between the mold wall and the solidified aluminum surface (air cavity/shrinkage), respectively. To evaluate the installation offset, a magnet with a smooth surface was employed to simulate the molten aluminum, serving as a second reflector by making contact with each side of the inner wall, as illustrated in Fig. 5(b). The experimental results were collected and presented in Fig. 5(c). Both EFPI-1 and EFPI-2 demonstrated minimal cavity length offsets of less than 22 μm. The total offset between the two channels was approximately 39 μm, which will be considered during the analysis of accurate gap measurements during aluminum casting. The measured results also indicate high stability, which is advantageous for meeting high-precision requirements.

IV. Results and Discussion

This section presents the results and observations of the aluminum pouring experiment, following the explanation of sensor operation theory, experimental design, and calibration results. The findings are summarized in Fig. 6. Aluminum casting serves as a prime example to illustrate the principles of heat transfer and thermodynamics. As depicted in Fig. 6(a), when molten aluminum is poured into the mold, heat is transferred to the surrounding materials, causing the aluminum to cool and solidify. During the solidification process, the aluminum undergoes a phase change from liquid to solid, releasing latent heat. This heat is transferred to the surrounding materials, causing them to heat up and expand. As the aluminum continues to cool and solidify, the heat transfer rate decreases, and the aluminum and surrounding materials begin to cool and contract, resulting in the generation of a gap. From a material science perspective, the phase change of aluminum from liquid to solid leads to a decrease in volume due to the formation of interatomic bonds. This volume reduction can induce dimensional changes and deformations in the final casting, which may pose challenges for applications requiring precise tolerances or complex geometries. Additionally, the result of the solidification process is a fully solidified aluminum casting that has acquired the shape of the mold, as illustrated in Fig. 6(b). The locations of the EFPI and RBS sensors are highlighted in red to indicate the positions where the sensors were installed. The collection of gap and temperature measurements commenced prior to the pouring of the molten aluminum and continued through partial cool-down.

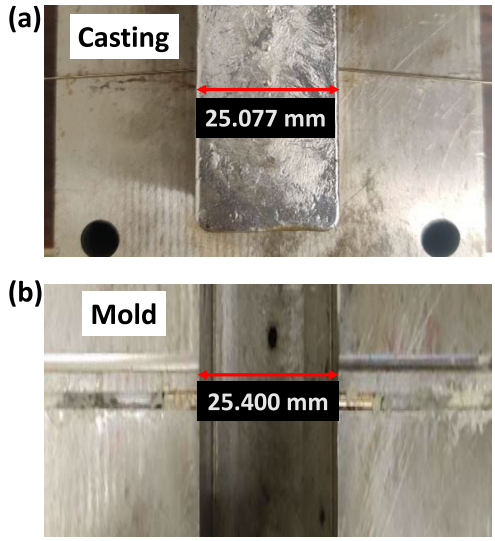

Fig. 7. Images of casting and mold. (a) Image of the aluminum casting, with a measured length of 25.077 mm. (b) Image of the empty mold, with a measured mold cavity length of 25.400. A 0.323 mm difference is observed indicating the aluminum shrinkage during solidification process.

The aluminum block was carefully removed from the mold after it had completely cooled down, and its length was measured to be 25.077 mm, as depicted in Fig. 7(a). A comparison was made with the length of the empty mold, which measured 25.400 mm, as illustrated in Fig. 7(b). The resulting difference of 0.323 mm indicates that the aluminum experienced shrinkage during the cooling process. This observation emphasizes the significance of considering shrinkage effects in casting design and production. By comprehending and effectively controlling the factors that contribute to shrinkage, such as alloy composition and cooling rate, it becomes feasible to minimize the impact of shrinkage and produce high-quality castings with the desired properties and dimensions.

To ensure accurate and reliable measurements, the Micron-Optics Hyperion SI-255 optical broadband interrogator was employed to capture interferograms at regular time intervals, as depicted in Fig. 8. The Hyperion SI-255 interrogator collected interferograms consisting of 20 000 points within a wavelength band of 1460–1620 nm. These interferograms were then processed using a custom low finesse EFPI demodulation algorithm to estimate the air gap in real-time. Data collection was carried out continuously for an average duration of one hour throughout the entire experiment, generating a comprehensive dataset for further analysis. The interferograms captured before the molten aluminum pouring are displayed in Fig. 8(a). Due to limitations of the integration system, the maximum measurable gap is only 3.5 mm, which is significantly smaller than the size of the mold cavity. As a result, the fringe visibility in the signal appears to be very low. To illustrate the change in cavity length and FSR during pouring, two interferograms from each EFPI were selected and are presented in Fig. 8(b). It is evident that the second reflection occurred when the aluminum surface was present, and an EFPI cavity was formed as soon as the aluminum was poured, resulting in the generation of the interferogram signal. Finally, to demonstrate the effect of solidification after pouring, two additional interferograms were chosen and are depicted in Fig. 8(c). The FSR value in Fig. 8(c) is lower than that in Fig. 8(b), indicating a longer cavity length according to (3). The comparison of the results from Fig. 8(b) and (c) confirms the solidification effect after pouring. Once the solidification process is complete, the aluminum ingot undergoes complete shrinkage, forming a constant EFPI cavity and an optical standing wave. The interferogram remains stable and consistent due to the unchanging cavity length. Advanced signal processing techniques are employed to analyze the interferograms and calculate the cavity lengths. These techniques involve zero-crossing and spectrum reconstruction to extend the measurement range to larger distances and improve measurement precision. By utilizing the zero-crossing technique, the location of the zero-crossing point in the signal can be accurately determined, serving as a reference for calculating the cavity length with high precision. The spectrum reconstruction technique helps eliminate phase noise, reducing measurement uncertainty. These advanced signal processing techniques extract important information about the cavity length and contribute to the overall accuracy of the measurement. With the use of these techniques, the EFPI system achieves a wider and more accurate measurement range of 10 μm to 3.5 mm, making it suitable for a broader range of applications. By employing this methodology, precise and detailed information regarding the gap changes during aluminum solidification was obtained, enabling a deeper understanding of the studied system, as depicted in Fig. 9. The demodulation results obtained from two EFPIs played a crucial role in understanding the shrinkage behavior of a molten aluminum cast part during cooling, which will be useful in steelmaking and continuous casting processes. The cavity length variations of EFPI-1 and EFPI-2 were measured and plotted against time, as shown in Fig. 9(a). EFPI-1 showed a change of 105.159 μm from the beginning of the experiment to 60 min, indicating that the aluminum had solidified. In contrast, EFPI-2 recorded a larger change of 254.691 μm within the same period. Moreover, a zoom-in plot was demonstrated the first minute of gap measurement during the aluminum solidification. When the molten aluminum is poured into the mold, it initially flows into the mold cavity and begins to fill the available space. As the aluminum material comes into contact with the mold surfaces, it tends to solidify and shrink quickly, resulting in the generation of the mold gap. The total shrinkage of the aluminum sample was then calculated, and the result was plotted in Fig. 9(b). The zoom-in plot provides a clear visualization of the initial shrinkage that occurs during the solidification process. Notably, within the first 0.3 min, a significantly higher rate of aluminum shrinkage is observed. This rapid shrinkage can be attributed to the abrupt phase change, viscosity change, and nucleation that take place during this early stage of solidification [1], [2]. Considering the 39 μm offset from the EFPI calibration test, an effective shrinkage measurement of 321 μm was obtained. This value closely matched the physical measurement value, with a small error of 2 μm. Achieving such high measurement accuracy is a significant accomplishment for steelmaking casting and represents a groundbreaking step in understanding the

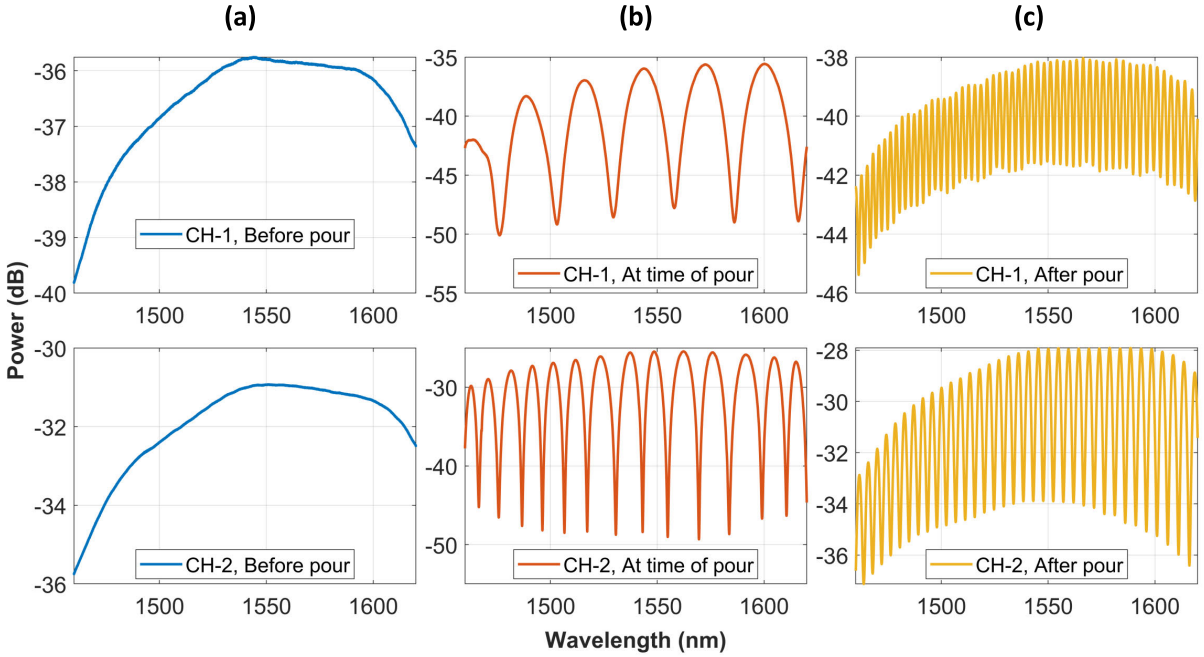

Fig. 8. Interferograms from two EFPIs at three experimental times throughout the molten aluminum casting process. (a) Interferograms captured before pouring. (b) Interferograms obtained during pouring. (c) Interferograms taken after pouring. The interferograms illustrate the behavior of the cavity length and fringe visibility as the molten aluminum is poured and solidifies. As the aluminum is poured, the interferogram shows the formation of the second reflector and the optical cavity. During solidification, the shrinking aluminum pulls away from the fiber end face, increasing the gap and causing a decrease in the FSR and fringe visibility.

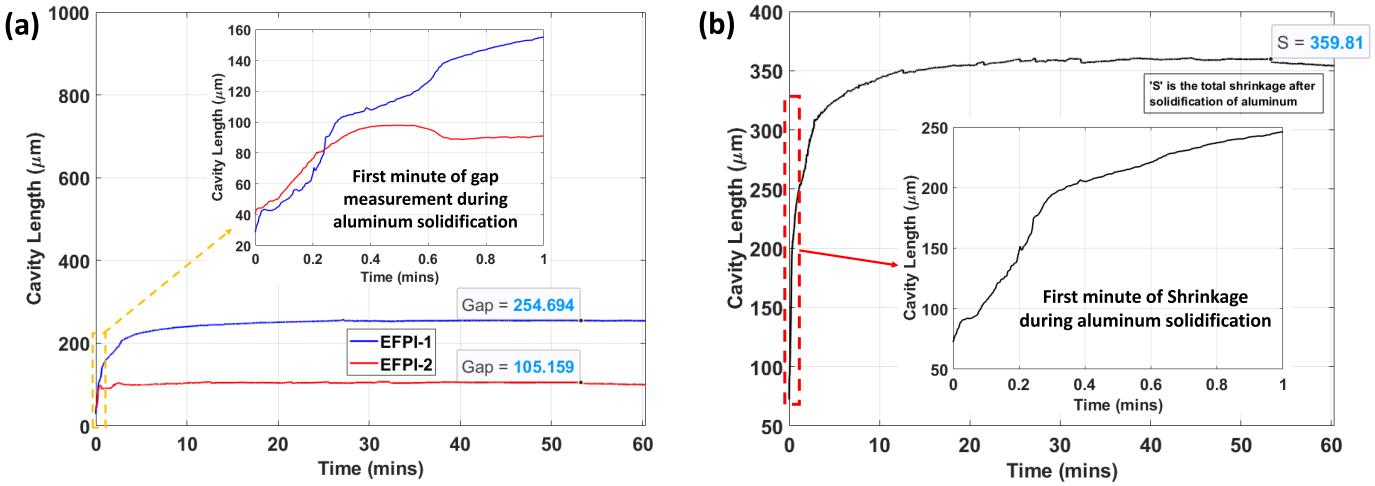

Fig. 9. Real-time cavity length measurements from both EFPIs and calculation of total shrinkage. (a) EFPI-1 and EFPI-2 showed a change of 105.159 and 254.694 μm from the beginning of the experiment to 60 min. The zoom-in plot was demonstrated the first minute of gap measurement during the aluminum solidification. (b) Total shrinkage, excluding the initial offset, was estimated to be approximately 360 μm. The zoom-in plot showed the first minute of shrinkage during the solidification process.

heat coefficient and aluminum shrinkage process, ultimately improving the quality of the casting process. With this level of accuracy, it is now possible to make more informed decisions about the casting process, leading to better outcomes in terms of product quality and reduced waste.

The temperature profiles in the mold cavity region were analyzed using RBS data, providing insights into the heat transfer dynamics during the casting process. Fig. 10 illustrates the spatial temperature profiles over time, revealing notable observations. Initially, upon pouring the molten aluminum into the mold, the maximum temperature was observed in the cavity region due to rapid heat transfer from the aluminum. As time progressed, the mold wall gradually heated up, resulting in a slower temperature increase in the cavity region. Interestingly, after approximately 6 min, the mold wall and cavity temperatures approached similar values, as indicated by the RBS data. This convergence suggests that the heat transfer from the aluminum to the mold was nearing completion, and the mold had achieved thermal equilibrium. This thermal equilibrium is critical for ensuring the production of high-quality cast products, as it facilitates uniform temperature distribution and consistent solidification throughout the mold.

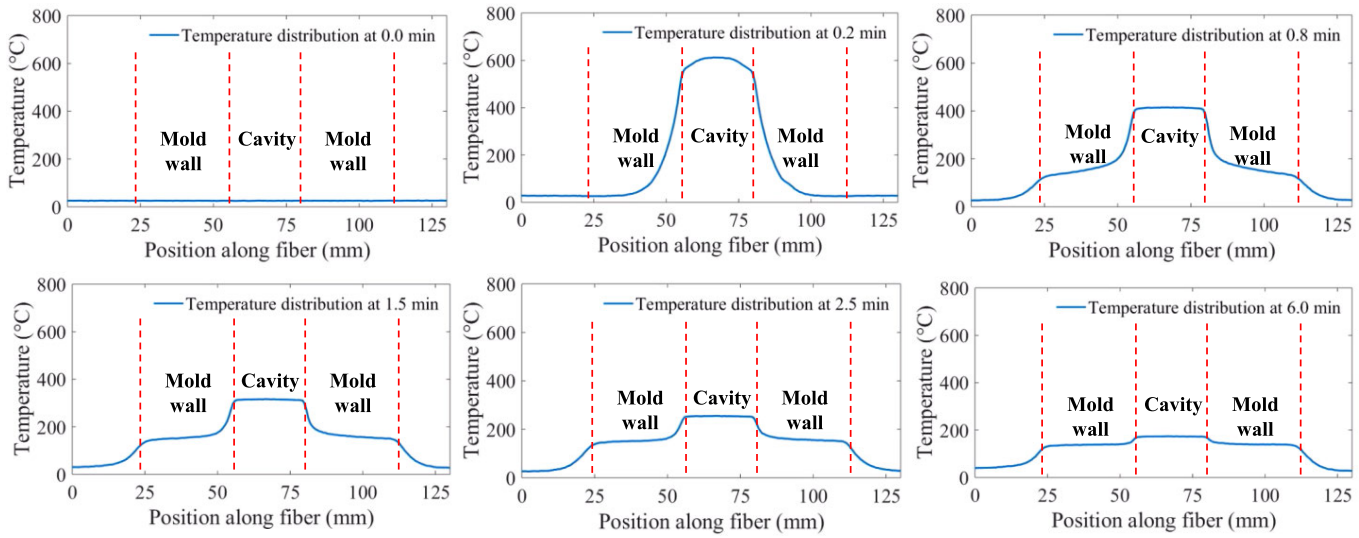

Fig. 10. Distributed temperature measurements using RBS for different time periods during the molten aluminum casting process. The graph displays the temperature distribution across the mold cavity region at multiple time intervals, offering a comprehensive visualization of the spatial temperature profiles during the casting process.

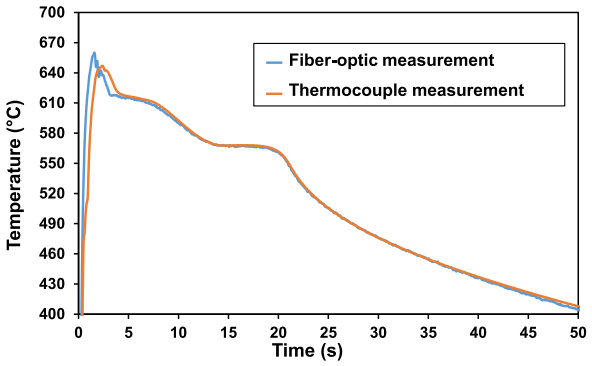

Fig. 11. Comparison of temperature measurements between the optical fiber (blue) and the thermocouple (orange) during the initial 50 s of measurement. The temperature profiles from both devices closely align (except for an interesting lag, see text), demonstrating the accuracy of the optical fiber measurement.

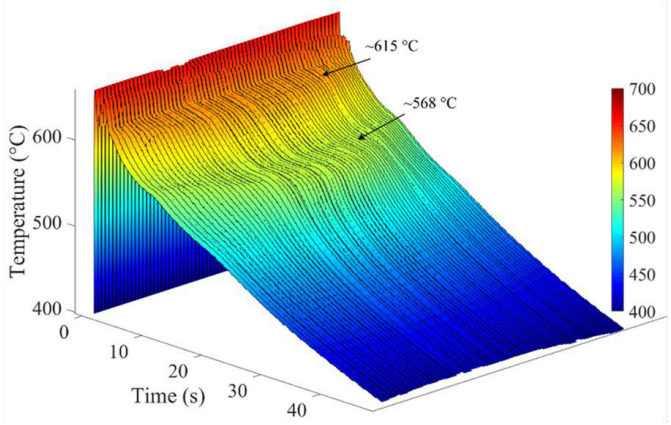

Fig. 12. Waterfall plot of spatiotemporal temperature data measured using fiber-optic sensor technology during an aluminum casting process. The plot represents a 3-D profile of temperature variations obtained from a 25.4 mm mold cavity, with measurements taken by an optical fiber starting from the moment the liquid metal was poured into the mold. The plot showcases the temperature distribution over both space and time, with a spatial resolution of 0.65 mm and a temporal resolution of 0.1 s.

The temperature profiles across the interface between the molten aluminum and the mold walls during the casting process were crucial to understanding the thermal behavior. The temperature data obtained from the optical fiber and thermocouple were processed and compared, as shown in Fig. 11. The comparison of the temperature readings allowed for an assessment of the accuracy and performance of the optical fiber measurement relative to the thermocouple. The temperature data from both devices exhibited close matching values, indicating that both the optical fiber and thermocouple accurately measured temperature. However, a slight lag was observed in the initial part of the temperature curves, suggesting that the optical fiber had a slightly faster thermal response compared to the thermocouple. This difference can be attributed to the varying thermal masses of the two devices. The thermocouple, with its larger thermal mass, required more time to respond to temperature changes, leading to a delay in the temperature readings compared to the optical fiber. As both devices reached thermal equilibrium, the temperature data exhibited a close match, demonstrating that both the thermocouple and optical fiber were capable of monitoring temperature in a dynamic environment. The consistency of the temperature data further confirmed the accuracy of the optical fiber measurement, indicating its potential as a reliable alternative to thermocouples for temperature monitoring in certain applications.

A comprehensive analysis of the temperature behavior during the entire experiment was performed by generating a detailed waterfall plot using the temperature distribution data measured by the optical fiber in the 25.42 mm mold cavity. Fig. 12 displays this waterfall plot, presenting the data acquired from the OFDR system with a spatial resolution of 0.65 mm and a temporal resolution of 0.1 s. The analysis of the plot revealed important insights into the temperature changes throughout the casting process. At the beginning of the plot,

a sudden jump in temperature was observed, indicating the moment when the molten aluminum was poured into the mold. Subsequently, a gradual decrease in temperature was observed as the aluminum transferred its heat to the mold. Notably, the plot highlighted uniform temperature arrests at 615 °C and 568 °C, corresponding to the primary and eutectic solidification stages of A356 aluminum. The end of the eutectic arrest marked the completion of the solidification process. Another significant observation from the plot was the variation in total solidification times across different locations within the mold. As anticipated, the total solidification times were shorter closer to the mold wall compared to the center of the casting. This valuable information can be utilized to optimize the cooling rate of the casting, ensuring a uniform and high-quality solidification process. The use of optical fiber technology for monitoring temperature profiles has proven to be an indispensable tool in ensuring the production of high-quality aluminum castings.

V. Conclusion

The results of this study have significant implications for the steelmaking industry, particularly in the context of aluminum casting processes. By successfully applying novel fiber-optic sensors to measure real-time mold gaps and thermal spatial profiles during the solidification of A356 aluminum, we have gained valuable insights into the heat transfer and cooling dynamics of the casting. The ability to monitor the gap between the mold wall and the casting surface using EFPI sensors provides crucial information for optimizing the casting process and ensuring the quality of the final product. The innovative use of molten metal as the second reflection interface for gap measurements, with a remarkably low measurement error of 2 μm, is a noteworthy contribution of this study. This approach offers a practical and accurate method for monitoring and controlling the gap evolution during solidification, which is essential for achieving uniform cooling and minimizing defects in the castings. Furthermore, the application of the RBS technique for real-time temperature measurements with a high spatial resolution of 0.65 mm provides detailed and precise data on interfacial heat transfer. This information is crucial for understanding the thermal behavior of the casting during solidification and optimizing the casting process parameters. By leveraging fiber-optic sensors, we can obtain accurate temperature profiles, enabling us to refine computer models of the casting process and improve our ability to predict and control solidification behavior. The practicality of using fiber-optic sensors in casting processes is demonstrated by the design of the mold system with unheated, uncoated tool steel. This design allows for easy installation of the optical fiber sensors, making it feasible to incorporate these sensors into existing casting setups without major modifications. The versatility and non-intrusive nature of fiber-optic sensors make them an attractive option for real-time monitoring of temperature and gap evolution in various casting processes, potentially revolutionizing the way we approach casting technology. Overall, the measured results obtained through the application of fiber-optic sensors provide a deeper understanding of interfacial heat transfer and solidification dynamics during aluminum casting. This understanding translates not only to improved aluminum casting processes but also has broader implications for the steelmaking industry. The knowledge gained from this study can be applied to develop improved casting technologies, optimize process parameters, enhance product quality and consistency, and even facilitate the production of previously incompatible alloys. By harnessing the power of fiber-optic sensors, we can advance the field of steelmaking and drive innovation in the manufacturing of high-quality cast products.

References

[1] A. J. Elliott, T. M. Pollock, S. Tin, W. T. King, S.-C. Huang, and M. F. X. Gigliotti, "Directional solidification of large superalloy castings with radiation and liquid-metal cooling: A comparative assessment," *Metall. Mater. Trans. A*, vol. 35, no. 10, pp. 3221–3231, Oct. 2004.

[2] A. J. Elliott and T. M. Pollock, "Thermal analysis of the Bridgman and liquid-metal-cooled directional solidification investment casting processes," *Metall. Mater. Trans. A*, vol. 38, no. 4, pp. 871–882, Apr. 2007.

[3] R. K. Nayak and S. Sundarraj, "Selection of initial mold–metal interface heat transfer coefficient values in casting simulations—A sensitivity analysis," *Metall. Mater. Trans. B*, vol. 41, no. 1, pp. 151–160, Feb. 2010.

[4] H.-C. Sun and L.-S. Chao, "An investigation into the effective heat transfer coefficient in the casting of aluminum in a green-sand mold," *Mater. Trans.*, vol. 50, no. 6, pp. 1396–1403, 2009.

[5] M. Trovant and S. A. Argyropoulos, "The implementation of a mathematical model to characterize mold metal interface effects in metal casting," *Can. Metall. Quart.*, vol. 37, nos. 3–4, pp. 185–196, Oct. 1998.

[6] P. S. S. Raju and S. P. Mehrotra, "Mathematical modeling of centrifugal casting of metal matrix composites," *Mater. Trans., JIM*, vol. 41, no. 12, pp. 1626–1635, 2000.

[7] A. Garcia, T. W. Clyne, and M. Prates, "Mathematical model for the unidirectional solidification of metals: II. Massive molds," *Metall. Trans. B*, vol. 10, no. 1, pp. 85–92, Mar. 1979.

[8] A. Fardi Ilkhchy, M. Jabbari, and P. Davami, "Effect of pressure on heat transfer coefficient at the metal/mold interface of A356 aluminum alloy," *Int. Commun. Heat Mass Transf.*, vol. 39, no. 5, pp. 705–712, May 2012.

[9] Y. Dong, K. Bu, Y. Dou, and D. Zhang, "Determination of interfacial heat-transfer coefficient during investment-casting process of single-crystal blades," *J. Mater. Process. Technol.*, vol. 211, no. 12, pp. 2123–2131, Dec. 2011.

[10] A. R. Baserinia, H. Ng, D. C. Weckman, M. A. Wells, S. Barker, and M. Gallerneault, "A simple model of the mold boundary condition in direct-chill (DC) casting of aluminum alloys," *Metall. Mater. Trans. B*, vol. 43, no. 4, pp. 887–901, Aug. 2012.

[11] M. Ahmadein, B. Pustal, N. Wolff, and A. Bührig-Polaczek, "Determination and verification of the gap dependent heat transfer coefficient during permanent mold casting of A356 aluminum alloy," *Materialwissenschaft und Werkstofftechnik*, vol. 48, no. 12, pp. 1249–1256, Dec. 2017.

[12] A. Tadesse and H. Fredriksson, "Experimental studies of gray cast iron solidification with linear variable differential transformer," in *Advances in the Science and Engineering of Casting Solidification*. New York, NY, USA: Springer, 2015, pp. 305–312.

[13] N. Wolff, B. Pustal, T. Vossel, G. Laschet, and A. Bührig-Polaczek, "Development of an A356 die casting setup for determining the heat transfer coefficient depending on cooling conditions, gap size, and contact pressure," *Materialwissenschaft und Werkstofftechnik*, vol. 48, no. 12, pp. 1235–1240, Dec. 2017.

[14] D. Crescini, A. Flammini, D. Marioli, and A. Taroni, "Application of an FFT-based algorithm to signal processing of LVDT position sensors," *IEEE Trans. Instrum. Meas.*, vol. 47, no. 5, pp. 1119–1123, Oct. 1998.

[15] G. Spiezia, R. Losito, M. Martino, A. Masi, and A. Pierno, "Automatic test bench for measurement of magnetic interference on LVDTs," *IEEE Trans. Instrum. Meas.*, vol. 60, no. 5, pp. 1802–1810, May 2011.

[16] M. Saari, B. Cox, E. Richer, P. S. Krueger, and A. L. Cohen, "Fiber encapsulation additive manufacturing: An enabling technology for 3D printing of electromechanical devices and robotic components," *3D Printing Additive Manuf.*, vol. 2, no. 1, pp. 32–39, Mar. 2015.

[17] C. Zhu, Y. Zhuang, B. Zhang, R. Muhammad, P. P. Wang, and J. Huang, "A miniaturized optical fiber tip high-temperature sensor based on concave-shaped Fabry–Pérot cavity," *IEEE Photon. Technol. Lett.*, vol. 31, no. 1, pp. 35–38, Jan. 1, 2019.
[18] D. Tosi, E. Schena, C. Molardi, and S. Korganbayev, "Fiber optic sensors for sub-centimeter spatially resolved measurements: Review and biomedical applications," *Opt. Fiber Technol.*, vol. 43, pp. 6–19, Jul. 2018.
[19] B. Zhang, R. E. Gerald, and J. Huang, "Miniaturized 7-in-1 fiber-optic Raman probe," *Opt. Lett.*, vol. 47, no. 21, p. 5561, 2022.
[20] C. Du, Q. Tang, J. Zhou, X. Guo, T. Yu, and X. Wang, "Fiber optic sensors based on photoacoustic effect for rebar corrosion measurement," *IEEE Trans. Instrum. Meas.*, vol. 68, no. 11, pp. 4559–4565, Nov. 2019.
[21] B. Zhang, H. Tekle, R. J. O'Malley, J. D. Smith, R. E. Gerald, and J. Huang, "In situ high-temperature Raman spectroscopy via a remote fiber-optic Raman probe," *IEEE Trans. Instrum. Meas.*, vol. 72, pp. 1–8, 2023.
[22] F. Mumtaz et al., "Thermally robust and highly stable method for splicing silica glass fiber to crystalline sapphire fiber," *Appl. Opt.*, vol. 62, no. 5, p. 1392, 2023.
[23] N. Sabri, S. A. Aljunid, M. S. Salim, and S. Fouad, "Fiber optic sensors: Short review and applications," in *Recent Trends in Physics of Material Science and Technology*. Singapore: Springer, 2014, pp. 299–311, doi: 10.1007/978-981-287-128-2_19.
[24] B. Zhang et al., "In situ and real-time mold flux analysis using a high-temperature fiber-optic Raman sensor for steel manufacturing applications," *J. Lightw. Technol.*, vol. 41, no. 13, pp. 4419–4429, Jul. 1, 2023.
[25] E. Schena, D. Tosi, P. Saccomandi, E. Lewis, and T. Kim, "Fiber optic sensors for temperature monitoring during thermal treatments: An overview," *Sensors*, vol. 16, no. 7, p. 1144, Jul. 2016.
[26] M. Ramakrishnan, G. Rajan, Y. Semenova, and G. Farrell, "Overview of fiber optic sensor technologies for strain/temperature sensing applications in composite materials," *Sensors*, vol. 16, no. 1, p. 99, Jan. 2016.
[27] F. Mumtaz, M. Roman, B. Zhang, and J. Huang, "Assembly-free ultra-sensitive miniaturized strain sensor based on an asymmetric optical fiber taper," *Measurement*, vol. 211, Apr. 2023, Art. no. 112655.
[28] J. M. Vaughan, "The plane Fabry–Pérot interferometer," in *The Fabry–Pérot Interferometers*. New York, NY, USA: Taylor & Francis, 2017, pp. 89–134.
[29] Y. Zhang, L. Yuan, X. Lan, A. Kaur, J. Huang, and H. Xiao, "High-temperature fiber-optic Fabry–Pérot interferometric pressure sensor fabricated by femtosecond laser," *Opt. Lett.*, vol. 38, no. 22, p. 4609, 2013.
[30] T. Wei, Y. Han, Y. Li, H.-L. Tsai, and H. Xiao, "Temperature-insensitive miniaturized fiber inline Fabry–Pérot interferometer for highly sensitive refractive index measurement," *Opt. Exp.*, vol. 16, no. 8, p. 5764, 2008.
[31] M. Nakazawa, "Rayleigh backscattering theory for single-mode optical fibers," *J. Opt. Soc. Amer.*, vol. 73, no. 9, p. 1175, 1983.
[32] S. T. Kreger et al., "High-resolution extended distance distributed fiber-optic sensing using Rayleigh backscatter," *Proc. SPIE*, vol. 6530, Apr. 2007, Art. no. 65301R.
[33] A. Yan et al., "Distributed optical fiber sensors with ultrafast laser enhanced Rayleigh backscattering profiles for real-time monitoring of solid oxide fuel cell operations," *Sci. Rep.*, vol. 7, no. 1, p. 9360, Aug. 2017.
[34] Z.-S. Liu et al., "Low-altitude atmospheric wind measurement from the combined Mie and Rayleigh backscattering by Doppler LiDAR with an iodine filter," *Appl. Opt.*, vol. 41, no. 33, p. 7079, 2002.
[35] M. Roman et al., "A spatially distributed fiber-optic temperature sensor for applications in the steel industry," *Sensors*, vol. 20, no. 14, p. 3900, Jul. 2020.
[36] J. C. Owens, "Optical refractive index of air: Dependence on pressure, temperature and composition," *Appl. Opt.*, vol. 6, no. 1, p. 51, 1967.
[37] C. Zhu et al., "A displacement sensor with centimeter dynamic range and submicrometer resolution based on an optical interferometer," *IEEE Sensors J.*, vol. 17, no. 17, pp. 5523–5528, Sep. 2017.

Bohong Zhang (Member, IEEE) received the Ph.D. degree in electrical engineering from the Missouri University of Science and Technology, Rolla, MO, USA, in 2022.

He is currently an Assistant Research Professor with the Lightwave Technology Laboratory, Department of Electrical and Computer Engineering, Missouri University of Science and Technology. His current research interests center around the advancement of optical and microwave sensors and instrumentation, focusing on their applications in intelligent infrastructures, biomedical sensing, and challenging environments.

Dr. Zhang is a member of IEEE, SPIE, OSA, and the Association for Iron and Steel Technology (AIST) organization.

Abhishek Prakash Hungund received the B.E degree in electronics and communication from Visvesvaraya Technological University (VTU), Karnataka, India, in 2015. He is currently pursuing the M.S. degree in electrical and computer engineering with the Lightwave Technology Laboratory, Missouri University of Science and Technology, Rolla, MO, USA.

His research is focused on the development of fiber optic-based interferometric sensors for air gap and thickness measurements of high-temperature substances, targeting continuous casting steel industries for quality improvement and process optimization. His research interests include microwave photonics and its application in the field of fiber optic sensor development.

Dinesh Reddy Alla received the M.S. degree in electrical engineering from the Missouri University of Science and Technology, Rolla, MO, USA, in 2017, and the B.Tech. degree in electronics and communication engineering from Jawaharlal Nehru Technological University, Kakinada, India, in 2014. He is currently pursuing the Ph.D. degree in electrical engineering with the Missouri University of Science and Technology.

His current research interests include distributed fiber-optic sensors for temperature and strain measurements.

Deva Prasaad Neelakandan received the B.E. degree in mechanical engineering from the Sri Shakthi Institute of Engineering and Technology, Coimbatore, India, in 2016, and the M.S. degree in mechanical engineering from the Missouri University of Science and Technology, Rolla, MO, USA, in 2018, where he is currently pursuing the M.S. degree in material science and engineering

His research interests include the instrumentation of optical fiber for temperature and strain measurements in steel-based applications.

Muhammad Roman received the Ph.D. degree in electrical engineering from the Missouri University of Science and Technology, Rolla, MO, USA, in 2022, and the M.S. degree in electrical engineering from the University of Engineering and Technology, Taxila, Pakistan, in 2013.

His current research interests include the development of fiber-optic and microwave photonic sensors and instrumentation for industrial applications.

Ronald J. O'Malley was the President of the Association for Iron and Steel Technology (AIST) from 2019 to 2021. He is currently the F. Kenneth Iverson Chair Professor of Steelmaking Technologies with the Department of Metallurgical Engineering, Missouri University of Science and Technology, Rolla, MO, USA. He is also the Director of the Kent D. Peaslee Steel Manufacturing Research Center (PSMRC), which is an industry-supported consortium with 19 industry members that support ∼U.S. $1M in research annually. He is also the PI for >U.S. $18M in research with the Department of Energy (DOE) and the Defense Logistics Agency (DLA) in areas of sensor development, hydrogen steelmaking, and electric furnace optimization. He is a Lecturer for several short courses in steel manufacturing, including the Brimacombe short course on continuous casting. He has more than 30 years of experience in the metals manufacturing industry at Alcoa, Alcoa Center, PA, USA, Armco/AK Steel, Middletown, OH, USA, and Nucor Steel, LLC, Decatur, AL, USA. He has authored more than 150 journal and conference proceedings papers, over 70 invited and contributed presentations, and holds three U.S. patents. His current research interests include H2 Ironmaking, electric arc furnace (EAF) steelmaking, steel refining, clean steel processing and inclusion engineering, steel-refractory interactions, continuous casting, deformation processing, sensor development for harsh steelmaking environments, and new steel grade development.

Dr. O'Malley is an AIST Distinguished Member and a fellow.

Laura Bartlett is currently the Robert V. Wolf Endowed Professor of metallurgical engineering and the Foundry Educational Foundation Key Professor of metal casting technology with the Missouri University of Science and Technology, Rolla, MO, USA. She is the Director of the Robert V. Wolf Educational and Research Foundry, Missouri University of Science and Technology and the Thermal Processing Laboratory. Her teaching and research experiences are in the areas of foundry steelmaking and the physical metallurgy of iron and steel casting alloys. Her work on the development of advanced high-strength and lightweight steels for military vehicles is currently funded by the Department of Defense through such organizations as the Army Research Laboratory and Defense Logistics Agency. She has coauthored more than 40 peer-reviewed articles. Her current research interests include the inclusion engineering and solidification phenomena in high-strength steels, the experimental and theoretical aspects of phase transformations, microstructure-mechanical property relationships in high-strength alloys, and the development of advanced high-strength and lightweight steels.

Dr. Bartlett has won several awards of distinction for her research including seven best paper awards and three research and professional development awards.

Rex E. Gerald II received the B.A. degree (Hons.) in chemistry from The University of Chicago (UC), Chicago, IL, USA, in 1984, and a conjoint Ph.D. degree in physical chemistry from the University of Illinois, Chicago (UIC), Chicago, and the Max Planck Institute (MPI), Heidelberg, Germany, in 1994.

He is currently a Research Professor with the Lightwave Technology Laboratory, Department of Electrical and Computer Engineering, Missouri University of Science and Technology (MS&T), Rolla, MO, USA. He holds 27 U.S. patents and coauthored more than 100 publications from research investigations conducted at UC, UIC, MPI, Argonne National Laboratory, and MS&T.

Jie Huang (Senior Member, IEEE) received the Ph.D. degree in electrical engineering from Clemson University, Clemson, SC, USA, in 2015.

He is currently the Roy A. Wilkens Endowed Associate Professor of electrical and computer engineering with the Missouri University of Science and Technology, Rolla, MO, USA. He has established the Lightwave Technology Laboratory (LTL), Rolla, with a strong track record of sustained research funding, high-quality journal publications, and state-of-the-art research infrastructures with cutting-edge capabilities. He has authored or coauthored over 100 refereed articles, 70 conference papers, one book chapter, and ten U.S. patent applications, all in the arena of advanced sensors. His current research interests include the development of optical and microwave sensors and instrumentation for applications in energy, intelligent infrastructures, clean environments, biomedical sensing, and harsh environments.